Mon. Not. R. Astron. Soc. **000**, 1–11 (2006) Printed 5 February 2008 (MN LATEX style file v2.2)

The Influence of Mass-Loss from a Star Cluster on its Dynamical Friction – I. Clusters without Internal Evolution

M. Fellhauer[1,2] ⋆, D.N.C. Lin[2] †
[1] *Institute of Astronomy, University of Cambridge, Madingley Road, Cambridge CB3 0HA, UK*
[2] *UCO/Lick Observatory, UC Santa Cruz, 1156 High Street, Santa Cruz, CA 95064, USA*

arXiv:astro-ph/0611557v1 17 Nov 2006

5 February 2008

ABSTRACT
Many Local Group dwarf spheroidal galaxies are found in the Galactic halo along great circles in the sky. Some of these stellar systems are thought to be the fragments of larger parent galaxies which have once intruded into and were torn apart by the tide of the Galaxy. Supporting evidences for tidal disruption are found in the form of stellar tidal bridges and tails along the orbits of some dwarf galaxies and globular clusters. In this study, we investigate the influence of mass-loss from star clusters or dwarf galaxies on the rate of their orbit decay due to the effect of dynamical friction. Using a series of numerical N-body simulations, we show that stars, which become unbound from their host-systems, but remain in their vicinity and share their orbits, still contribute to the mass responsible for the dynamical friction. As a rule-by-thumb, the magnitude of dynamical friction at any instance can be approximated by the bound mass plus half of the mass which has already become unbound during the proceeding Galactic orbit. Based on these results, we suggest the tidal disruption of relatively massive satellite stellar systems may be more abrupt than previously estimated.

Key words: methods: N-body simulations — galaxies: star clusters — galaxies: dwarf — galaxies: kinematics and dynamics

1 INTRODUCTION

In the widely adopted ΛCDM scenario, large normal galaxies are formed through the mergers of much smaller entities, dwarf galaxies (Blumenthal et al. 1984; Navarro, Frenk & White 1995). In the halo of the Galaxy, hundred of such entities are anticipated (Moore et al. 1999), far exceed the previously known satellite stellar systems. In recent years, however, many new satellite dwarf spheroidal galaxies are being discovered, namely Ursa Major (UMa; Wilman et al. 2005), Canes Venatici (CanVen; . 2006a), Bootes (Boo; Belokurov et al. 2006b) and Ursa Major II (UMa II; Zucker et al. 2006b). The study of their dynamical evolution and star formation history has becoming an important aspect in the determination of poorly known halo structure and the development of galaxy formation theory.

As they orbit around the halo of their host galaxies, satellite galaxies encounter the effect of dynamical friction and undergo orbital decay. When they migrate toward the centre of their host galaxy, the increasingly intense background tidal perturbation leads to the disruption of loosely bound satellites. In the vicinity of several satellite galaxies, streams of escaping stars have been discovered (e.g. Belokurov et al. 2006a). Similar tidal debris is also found along the orbits of some loosely bound globular clusters (Odenkirchen et al. 2003; Belokurov et al. 2006c).

As a theoretical construct, the dynamical-friction process was first described by Chandrasekhar (1943). Under the idealised assumption that an undisruptable stellar system moving through a homogeneous background of stars (with a Maxwellian phase space distribution and an isotropic velocity dispersion), the magnitude of dynamical friction is proportional to the mass of the system. But, for disintegrating stellar systems with a declining mass within their tidal radii, it remains uncertain whether this mass includes the contribution from those stars or gas which became gravitationally detached during the most recent passages. In principle, their gravity continues to exchange momentum with the background constituents. However, their weakened gravitational coupling with their originally parent galaxies also reduces the rate of momentum transfer between them.

The efficiency and outcome of this mass-loss process are sensitively determined by the nature and magnitude of the dynamical friction. If the orbital decay rate is directly proportional to the mass of the residual stars which remain gravitationally bound to the sinking and disrupting satellite stellar systems, their cores' migration would be quenched and structure would be preserved as their outlying stars become detached. In an attempt to account for its stellar metallicity dispersion, it has been proposed that the globular cluster ω-Centauri may indeed be the core-remnant of a destroyed satellite dwarf spheroidal galaxy (Tsuchiya et al. 2004;

⋆ madf@ast.cam.ac.uk
† lin@ucolick.org

Bekki & Freeman 2003; Hilker & Richtler 2000). If, however, the relative rapid orbital decay rate is sustained despite the tidal disruption of the satellite dwarf galaxies or globular clusters, they would completely disrupt and their constituent stars would add to the stellar components of the outer halo in form of streams (Ibata et al. 2002; Martinez-Delgado 2004).

Dynamical friction is a process which also plays a crucial role in other stellar-dynamical problems. Recent observations of the Galactic Centre, for example, revealed very young star clusters, with ages of a few Myr, inside the inner parsecs of our Galaxy (Tamblyn & Rieke 1993; Krabbe et al. 1995; Gerhard 2001). Because this location is believed to be too hostile to form star clusters, these objects must have formed further out and have sunk to the actual position within their short lifetime. The mechanism to shrink their orbit is dynamical friction (Chandrasekhar 1943). Once again, whether the rate of orbital decay is affected by the tidal disruption of the clusters determines the fate of these stellar systems.

The above discussions indicate that theoretical and numerical studies to establish a better understanding of dynamical friction are important tasks. Recent numerical studies on this topic focused on the influence of resolution of the used N-body codes on the results of dynamical friction (Spinnato et al. 2003), the influence of the density profile on the Coulomb logarithm (Penarrubia et al. 2004; Just & Penarrubia 2005) or the influence of the mass-loss on the orbital decay (McMillan & Portegies Zwart 2003; Fujii et al. 2006).

In this paper, we investigate the interplay between dynamical friction, which leads to the sinking of the object, and the mass-loss due to tidal heating by means of numerical N-body simulations. The overall objectives of this investigation are similar to those motivated the investigation by Fujii et al. (2006). But, in our simulations, we follow the evolution of the satellite further, beyond the stage of complete disruption. We also take into account the artificial effects of resolution limitations of N-body codes and the variation of $\ln\Lambda$ with distance to the centre of the background. In the next section we briefly recapitulate the standard theory of dynamical friction followed by the setup of our N-body models. In section 4 we present the results of our calculations in a systematic manner. According to the conventional formula for dynamical friction, the rate of orbital evolution is determined by the product of the effective mass ($M_{\rm cl}$) of the satellite and a parameter ($\ln\Lambda$) which measures the spacial extent of the halo region which effectively responds to the satellite's gravity. In order to disentangle these two effects, we first carry out an idealised simulation on the orbital evolution of a cluster with a point-mass potential and a constant mass. We show that the magnitude of $\ln\Lambda$ artificially depends on the numerical resolution for close encounters in this idealised model. However, this particular model over-estimated the importance of close encounters. In order to consider a potential with a more realistic mass distribution, we also carry out a simulation for a cluster based on a Plummer model. We consider the case of a compact cluster so that its mass is preserved over several orbital periods. We show that due to the "soften" nature of the cluster's potential, the magnitude of $\ln\Lambda$ is slightly below that deduced for the cluster with a point-mass potential (see also Spinnato et al. 2003). Together, these simulations demonstrate the validity for the numerical method in its ability to resolve the gravity over close stellar encounters.

We present evidences that the unbound, recently torn stars along the tidal tails also contribute to the dynamical friction on the cluster's orbital evolution. We present the simulation of a loosely bound cluster which is undergoing total disruption. With the simulation of this disintegrating cluster and another idealised model for an unbound moving cluster, we present evidence that the unbound but nearly co-moving stars contribute to the orbital decay of the residual core. We summarise our results and discuss their implications in section 5.

2 DYNAMICAL FRICTION

The mechanism to shrink the orbits of star clusters or dwarf galaxies in the tidal field of their host-galaxy is dynamical friction, which was studied first theoretically by Chandrasekhar (1943). In his formula

$$\frac{d\mathbf{v}_M}{dt} = -\frac{4\pi\ln\Lambda G^2\rho M_{\rm cl}}{v_M^3}\left[\mathrm{erf}(X)-\frac{2X}{\sqrt{\pi}}\exp(-X^2)\right]\mathbf{v}_M \quad (1)$$

for $M_{\rm cl}\gg m$ where $X=v_M/\sqrt{2}\sigma$, v_M is the velocity of the object with mass $M_{\rm cl}$, ρ is the mass density of the surrounding material, m is the typical single mass and σ the typical velocity dispersion of the surrounding medium, Λ describes the ratio of the largest to the smallest impact parameter:

$$\Lambda = \frac{b_{\rm max}v_M^2}{G(M_{\rm cl}+m)} = \frac{b_{\rm max}}{b_{\rm min,theo}}. \quad (2)$$

This parameter varies with the different environments and the determination of $\ln\Lambda$ is a crucial point in determining the sinking time scales. Even though Chandrasekhar's formula is only a linear approximation and derived for an infinite, homogeneous background, numerical studies proved that the formula holds also for 'realistic' backgrounds (Binney & Tremaine 1987; Hasimoto et al. 2003).

We determine $\ln\Lambda$ from the sinking rate in a background medium in which the mass distribution follows a power law profile

$$M_{\rm back}(D)=A\cdot D^{\alpha}, \quad (3)$$

where D is the distance from the centre of the background medium. For this mass distribution, we can determine the evolution of a satellite's orbit with the analytical formula derived by McMillan & Portegies Zwart (2003):

$$D(t) = D_0\left[1-\frac{\alpha(\alpha+3)}{\alpha+1}\sqrt{\frac{G}{AD_0^{\alpha+3}}}\times \left(\mathrm{erf}(X)-\frac{2X}{\sqrt{\pi}}\exp(-X^2)\right)M_{\rm cl}\ln\Lambda t\right]^{\frac{2}{3+\alpha}}. \quad (4)$$

Here we denote $D(t)$ as the satellite's distance from the centre of the background medium. We utilise this equation below to deduce the magnitude of $(M_{\rm cl}\ln\Lambda)$ from the value of $D(t=0)=D_0$ and $D(t)$.

In a recent numerical study, Spinnato et al. (2003) investigated the in-fall of a point-mass into the Galactic centre and compared the results of different numerical schemes. In this point-mass case the sinking of the massive particle was limited by the resolution of the used N-body codes, which in the case of a particle-mesh code is given by the length of one cell l:

$$b_{\rm min} \approx b_{\rm min,theo}+l \quad (5)$$

By fitting their results with varying resolutions they determined that the maximum impact parameter is approximately half the distance to the Galactic Centre ($a'\approx 0.5$):

$$b_{\rm max} = a'\cdot D \quad (6)$$

Another important outstanding issue concerning the Chandrasekhar's formula for the dynamical-friction efficiency in Eq. 1 is the specification of the mass $M_{\rm cl}$ of the sinking stellar system. In contrast to a sinking massive particle with fixed mass M, a star cluster experiences tidal heating and internal evolution, leading to a significant mass-loss during its life-time until it is totally disrupted. For such stellar systems, the constant mass in Eq. 1 has to be replaced by a time-dependent expression. But stars which become unbound to their parent clusters do not disperse immediately. They continue to travel on almost identical orbits as the parent cluster itself and disperse only slowly with time. The question we want to address in this project is whether these stars are still taking part in the dynamical friction of the whole cluster and to which extend or if only the bound particles contribute to the sinking of the star cluster.

model	D_0	$r_{\rm pl}$	$r_{\rm t,ini}$	orbit
4.1	2.78	point mass	—	circular
4.2	2.78	0.05	0.25	circular
4.3	2.78	0.10	0.25	circular
4.4	2.78	0.05	(0)	circular
4.5a	2.78	point mass	—	eccentric $\epsilon = 0.4$
4.5b	2.78	0.05	0.25	eccentric $\epsilon = 0.4$

Table 1. Model parameters of our simulations. First column gives the section in the manuscript in which the simulation and its results are explained, D_0 is the initial distance to the centre of the background, $r_{\rm pl}$ is the initial Plummer radius with the initial cut-off radius being $5r_{\rm pl}$. $r_{\rm t,ini}$ is the initial tidal radius, which is not applicable to the point mass simulations and the simulation 4.4 where the self-gravity is artificially switched off. Last column gives the adopted orbit. In the eccentric orbit case D_0 is the initial apo-centre of the simulation. The initial mass in all simulations is 1.0 and the cluster is modelled with 1,000,000 particles in all cases except the point mass runs.

3 NUMERICAL METHODS AND MODEL PARAMETERS

As prescription for the background galaxy we adopt the model of a lowered isothermal sphere (e.g. Binney & Tremaine 1987). For computational convenience, we adopt normalised computer units in which the mass distribution is cut off at $D_{\rm cut} = 10.0$. We also set the total mass of the background galaxy to be $M_{\rm tot} = 1000.0$. Finally, we specify $G = 1$ in model units which implies a theoretical constant circular velocity of $V_0 = 10.0$ and a characteristic dynamical time $T_{\rm cr} = 1.414$. The background is represented with such a phase space distribution among 5,000,000 particles.

The star cluster is modelled as a Plummer sphere with $M_{\rm pl} = 1.0$ and a Plummer radius $r_{\rm pl}$. The density distribution of the Plummer sphere is truncated at $r_{\rm cut} = 5r_{\rm pl}$. In order to enhance the mass resolution of the cluster, we use 1,000,000 particles to represent the stars in the cluster models. Even though the adopted mass-ratio (10^{-3}) between the satellite and background is more appropriate for simulating the interaction between dwarf galaxies and their host galaxies, we use the generic term 'star cluster' or 'cluster' for our object throughout the text. An overview of the cluster parameters used in the different sections of this manuscript is given in Tab. 1.

For the numerical simulations, we use a particle-mesh code named SUPERBOX (Fellhauer et al. 2000) to compute the gravitational interaction between particles. This scheme has two levels of higher resolution sub-grids focusing on the centres of the simulated objects (here background and star cluster). During the simulation, stars which are attached to the star cluster travel within the medium-resolution grid of the background with a cell-length of $l = 0.08$. The innermost grid with the highest resolution covers the central area of the background until $D = 1$ with a resolution of 0.016. The time-step of the simulation is adjusted that particles with typical velocities do not travel more than one grid-cell per time-step which gives a time-step of ${\rm dt} = 0.001$. Particle-mesh codes are designed to suppress the effect of two-body relaxation in galaxy simulations because their characteristic time scales are longer than a Hubble time. Therefore, despite the limited number of representative particles, a star cluster simulated with SUPERBOX do not artificially generate any internal dynamical evolution such as mass segregation or core collapse.

The background model is first set-up and integrated forward for several dynamical times to have the numerical particle distribution adjust to the used grid-code with its resolutions. This initial relaxation alters the shape of the mass-profile of the background mainly in its innermost central part and in the outer envelope. After this initial adjustment, we determine the profile and the half-mass radius. Around the half-mass radius, the profile continues to be nearly isothermal.

The presence of the stellar cluster is introduced to the background particles by inserting an analytical Plummer-potential with growing mass and a prescribed Plummer-radius according to the subsequently used star cluster model. The initial orbit of the cluster is assumed to be circular with a radius equal to the half-mass radius of the background. This computational procedure is carried out in order for the particles representing the background to adjust adiabatically to the later inserted star cluster and to avoid spurious reactions of the background when the star cluster is inserted. In reality, such adjustment is expected since most satellite stellar systems were probably not formed *in situ*. In all our simulations, we also ensure a similar adiabatic adjustment for the stellar distribution within the clusters. The model of the star cluster is also first simulated separately to have its internal particles to adjust to the numerical grid-structure. Finally the "live" star cluster is inserted in exchange to the analytical Plummer-potential at the half-mass radius with the actual measured circular velocity.

4 COMPUTATIONAL RESULTS

4.1 The orbital evolution of a cluster with a constant point-mass potential

In order to disentangle the effect of a changing $\ln\Lambda$ versus that of a changing mass $M_{\rm cl}$ in Chandrasekhar's formula, we first simulate the orbital decay of a cluster with a point-mass potential and a total mass $M_{\rm pm} = 1.0$. This simulation provides a determination on the largest value of $\ln\Lambda$. With the specified resolution of our code, this determination is possible because the simulated dynamical friction efficiency is resolution limited for a point-mass potential whereas $b_{\rm min}$ is proportional to the characteristic length scales of extended satellite systems which is generally larger than the resolution.

The star cluster is inserted at the half-mass radius which in our case is $D_0 = 2.78$. The characteristic orbital period at the half mass radius is ≈ 1.75. Fitting a power law of the form of Eq. 3 in the range $D \in [1.0 : 3.5]$ to the background gives $A = 189.9 \pm 0.6$ and $\alpha = 0.935 \pm 0.003$. Inserting these values in Eq. 4 and applying that the velocity of the star cluster is exactly the measured circular velocity at this radius, leads to the following theoretical expression

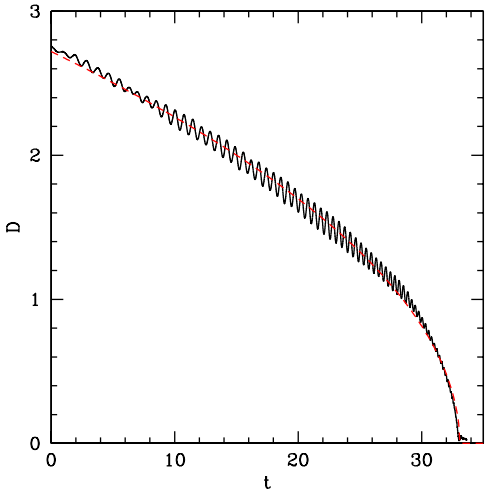

Figure 1. The orbital decay of a cluster modelled as a point-mass potential. Shown is the distance D vs. the time. The dashed line (red on-line) shows the fitting curve using a single $\ln\Lambda$ according to Eq. 7

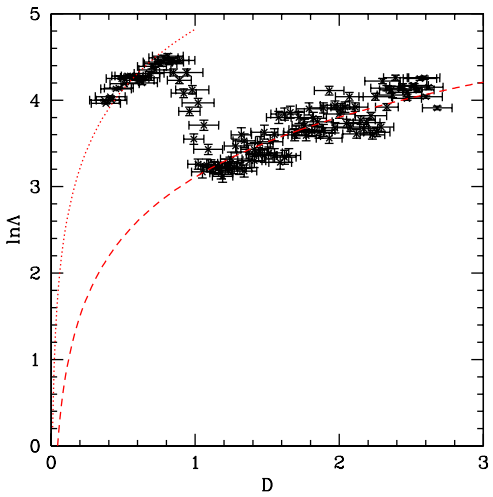

Figure 2. Fitting values of $\ln\Lambda$ for each 5 periods of oscillations against mean distance D. Lines (red on-line) are the fitting curves for the different grid resolutions (dashed: medium resolution; dotted: high resolution) as described in the main text.(see Eq. 10-12)

for the orbital evolution,

$$D(t) = D_0\left(1.0 - \frac{0.059}{D_0^{1.97}} M_{\rm cl}\ln\Lambda t\right)^{0.51}. \quad (7)$$

In the above expression, $D(t)$ is a function of $(M_{\rm cl}\ln\Lambda)$. We can break this degeneracy with our idealised model in which the cluster is assumed to have a constant ($M_{\rm cl}=1$ at all times). We consider D_0 as a fitting parameter because even with the initial orbit of the star cluster specified to match the circular velocity of the background, small amplitude oscillation in D during its orbital decay occur. This oscillation is due to the discreteness of the time-step and the 'granularity' of the background. We reduced these numerical oscillations as much as possible but small and slowly growing epicyclic oscillations around the expected analytical orbits (Theis, private communication) remain. This numerical artifact does not affect our overall results.

Using the implementation of the nonlinear least-squares (NLLS) Marquardt-Levenberg algorithm in *gnuplot*, we find that the orbital evolution obtained from the numerical simulation (as shown in Fig. 1) can be fitted with the analytic expression from Eq. 7 with

$$D_0 = 2.7174 \pm 0.0003 \quad (8)$$
$$\ln\Lambda = 3.655 \pm 0.001. \quad (9)$$

This result is in good agreement with the previous study of Spinnato et al. (2003) with respect to the dependence of $b_{\rm min}$ and therefore $\ln\Lambda$ on the resolution of the code (see Eq. 5). The values of $b_{\rm max} = a' \cdot D_0$ however differ from the findings in the previous study. While Spinnato et al. (2003) found values of a' in the range of 0.4 to 0.6 our result implies $a' \approx 1.2$. A possible reason is that Spinnato et al. (2003) left $b_{\rm min,theo}$ as a free parameter to fit their results and deduced a value which is three times lower than expected by Eq. 2. Furthermore in both studies the background was not perfect isothermal introducing a slight dependence of $b_{\rm min,theo}$ with distance.

In order to examine if $\ln\Lambda$ evolves with distance to the centre of the background, we now take only values from one maximum (minimum) of the curve to the 5th next maximum (minimum) and again fit Eq. 7 to all the time-slices available. The measured values of $\ln\Lambda$ are plotted in Fig.2 against their mean distance D during the used time interval. The values of $\ln\Lambda$ clearly decrease with the distance to the centre.

In Section 2, we discussed the dependence of $\ln\Lambda$ on the numerical resolution for a cluster with a point-mass potential (see Eq. 5). In order to test this dependence, we show also the results of the smallest cell length size l of the highest resolution grid interior to $D = 1.0$. The results of our numerical simulation clearly show a jump in the value of $\ln\Lambda$ at $D = 1.0$ when the cluster with a point-mass potential enters the simulation area with the highest resolution. We applied the following fitting formula to the data

$$\ln\Lambda = \ln(b_{\rm max}) - \ln(b_{\rm min}) = \ln(a\cdot D) + b \quad (10)$$

where a and b are two constants. If $b_{\rm min} = b_{\rm min,theo} + l$ the values of b would be 2.458 in the region $D > 1.0$ and 3.829 in the region $D < 1.0$. Using again the NLLS algorithm of *gnuplot* we obtain the following results for a and b (values for $D < 1.0$ are given in brackets):

$$a = 1.92 \pm 0.03 \ \ (2.68 \pm 0.06) \quad (11)$$
$$b = 2.46 \pm 0.02 \ \ (3.83 \pm 0.02). \quad (12)$$

The values for b are in very good agreement with the predicted values derived from Eq. 5. The values for a differ from the results of a' and the study by Spinnato et al. (2003), because in these cases a global $\ln\Lambda$ was used to fit the entire orbital decay curve. The two independent fitting curves are shown as the dashed (dotted) line in Fig. 2. We use the dashed fitting line for the examination of the results in the live star-cluster simulations. The values for $\ln\Lambda$ derived for a cluster with a point-mass potential with the given resolution of the code should be systematically larger than the values of $\ln\Lambda$ expected for an extended star cluster but at least we get an upper

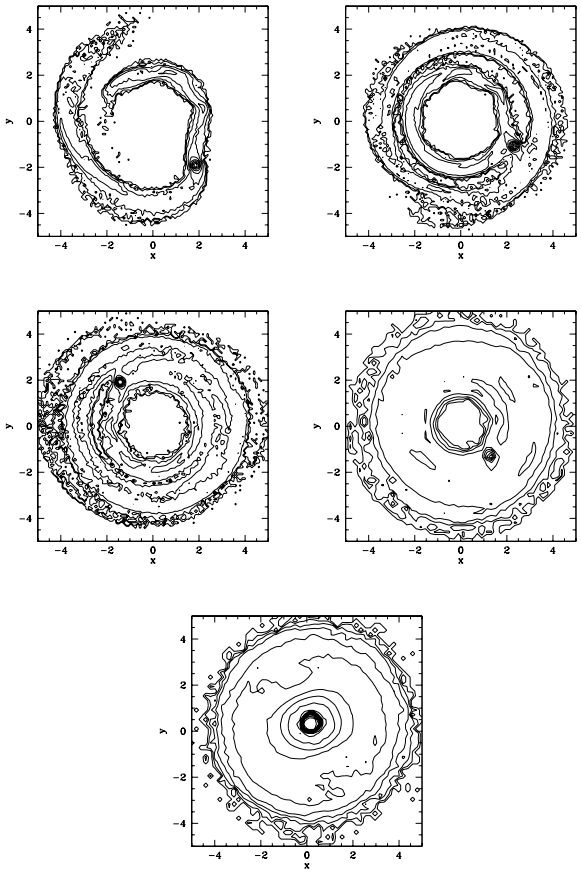

Figure 3. Contour-plots of the time-evolution of the sinking star cluster (smaller than the tidal radius). Shown are the time-steps 2.5, 5.0, 10.0, 20.0 and 40.0.

limit for $\ln\Lambda$ which should provide us with a lower limit on the mass taking part in the dynamical friction process.

4.2 A compact star cluster with a size smaller than its tidal radius

Typical satellites have extended mass distribution. For example, the internal density distribution within dwarf spheroidal galaxies is relatively flat. The half mass radii of many loosely bound globular clusters are significant fraction of their tidal radii. Globular clusters near the Galactic centre such as the Arches cluster also have relatively flat density profile. The characteristic velocity dispersion within these systems are closer to that of truncated isothermal sphere than that for a point mass potential. In order to simulate a more realistic potential for typical satellites, we adopt a model in which a cluster is represented by 10^6 particles with a Plummer-model phase-space distribution.

We place this star cluster at the same half-mass radius of the background galaxy as in the previous simulation for a cluster with a point-mass potential. We deduce the magnitude of the cluster's tidal radius analytically using formula 7-84 from Binney and Tremaine (1987). We set the Plummer radius to be $r_{\rm pl} = 0.05$. With a total mass 1.0, the analytic tidal radius at D_0 is ~ 0.25. In this simulation, our objective is to examine whether the magnitude of $\ln\Lambda$ for a realistic cluster potential differ significantly from that for a point-

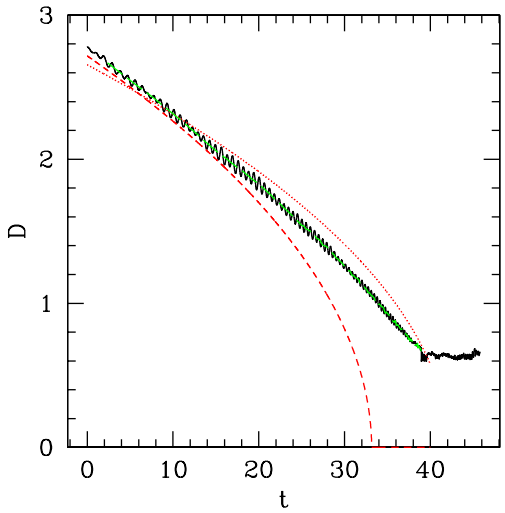

Figure 4. The orbital decay of a compact stellar cluster which is smaller than its tidal radius. Shown is the distance D of the star cluster to the centre of the background vs. time (solid line; black on-line). The short dashed line (red on-line) shows the fitting curve derived for the point-mass case ($M_{\rm cl} = 1.0 = const.$) and the dotted line (red on-line) shows a fit of Eq. 7 to the whole curve, i.e. trying to fit a constant $M_{\rm cl}\ln\Lambda$. As expected these two curves do not fit the data properly. The long dashed line (green on-line) which is barely visible because it fits the data almost exactly is again Eq. 7 but this time the actual values for $M_{\rm cl}\ln\Lambda$, as determined below, are inserted.

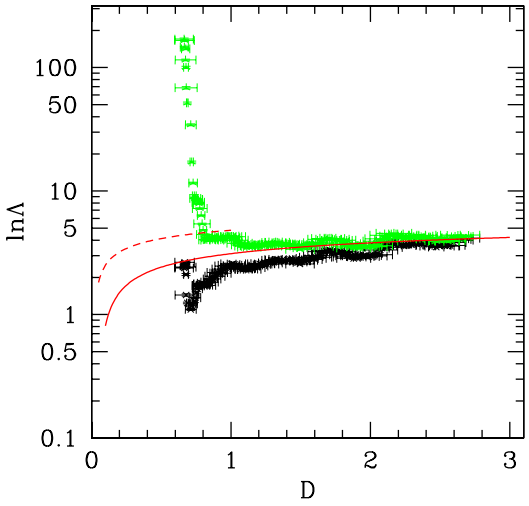

Figure 5. The magnitude of $\ln\Lambda$ associated with the orbital decay of a compact stellar cluster due to dynamical friction. The values of $\ln\Lambda$ are derived for each 5 oscillations. Crosses (black on-line) are deduced under the assumption of a constant total mass ($M_{\rm cl} = 1.0$) of the cluster (see Eq. 13). The tri-pods (green on-line) are derived under the assumption that only the bound mass contribute to the dynamical friction (see Eq. 14). The solid and dashed lines (red on-line) are the fitting curves for $\ln\Lambda$ derived from the point-mass potential case.

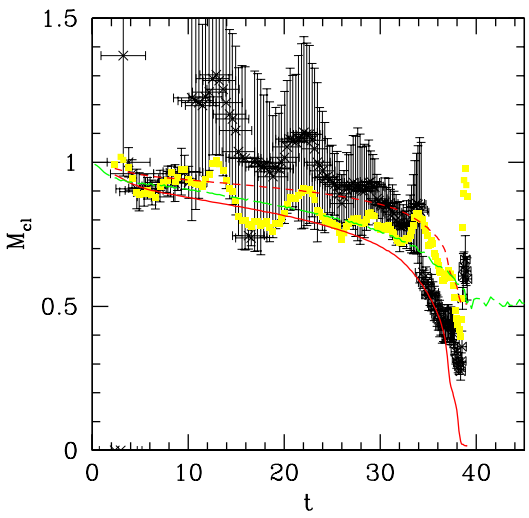

Figure 6. Mass evolution of the star cluster smaller than the tidal radius. Solid line (red on-line) is the bound mass of the cluster as calculated by SUPERBOX. Crosses (black) and squares (yellow) denote the mass of the cluster which takes part in the dynamical friction if we insert the point-mass values of $\ln\Lambda$ in Eq. 7 and solve for the cluster mass. For the crosses we take the measured values; for the squares the values derived with the fitting curve from Fig. 2. The short dashed line (red) shows the bound mass of the cluster plus the mass which is spread along the orbit in a torus of the size of the cluster around the galaxy and only particle with the same velocity signature (orbital velocity plus/minus initial velocity dispersion) as the cluster are taken into account. Long dashed line (green) is our rule-by-thumb: bound mass plus half the unbound mass.

mass potential. In order to make this comparison with the previous model, we consider a cluster which is expected to be well preserved at least for several galactic orbital periods. In order to guarantee that the total mass of this cluster is initially within its tidal radius, we introduce a cut off in the stellar density at $r_{\rm cut} = 0.25$.

The results of this simulation at five epochs are shown in Fig. 3 (see also Fig. 6). These figures indicate that, due to tidal heating, the cluster looses mass only slowly with time. The cluster is therefore able to migrate deeply into the potential of the host galaxy. Fig. 4 shows the evolution of the star cluster distance from the centre, D. The dotted line shows a fit to the orbit-decay curve for all data-points, while the dashed line gives the fitting line which is derived from the cluster model with a point-mass potential. It is evident that none of these lines provides an excellent approximation of the data-points.

Following the same procedure as in the model with the point-mass potential, we now determine the combined values of $M_{\rm cl}\ln\Lambda$ for the small time-slices. While the bound mass, the time and distance of the cluster are instantaneous quantities which are determined at each time-step, the combined quantity $(M_{\rm cl}\ln\Lambda)(t)$, determined via the sinking rate using Eq. 7, can only be accessed in a time-average approximation. Although all quantities evolve over finite time-spans, we evaluate the magnitude of $(M_{\rm cl}\ln\Lambda)(t)$ with the mean values for the time, distance and bound mass. An optimised time interval is chosen so that it is sufficiently short to ensure that the instantaneous quantities do not evolve significantly while it is adequate to limit the uncertainties in the estimated sinking rate during each of these time intervals. This simple-to-use approach introduces modest error bars in several figures throughout our manuscript.

The results are plotted in Fig. 5. The crosses represent the value of $\ln\Lambda$ obtained under the assumption of constant $M_{\rm cl} = 1.0$:

$$\ln\Lambda(t)_{\rm crosses} \quad = \quad (M_{\rm cl}\ln\Lambda)(t) \;/\; M_{\rm bound}(t=0) \qquad (13)$$

In Fig. 5, the crosses fall slightly below the fitting line for the cluster with a point mass potential (which is represented by the dashed line). This disparity is expected since an extended object should have a larger $b_{\rm min}$ than that with a point-mass potential. For $t < 30$ or $D > 1$, the difference between these two simulation is less than 20%. But, it is also visible that the deviation from the fitting line grows with time, especially at $t > 30$ (or equivalently as D decreases below 1). This growing difference is due to lost of mass from the stellar cluster. This divergence shows that a constant $M_{\rm cl}$ approximation does not adequately represent the results of the simulation.

The tri-pods in the same figure represent the values of $\ln\Lambda$ derived under the assumption that only the bound mass is responsible for dynamical friction:

$$\ln\Lambda(t)_{\rm tri-pods} \quad = \quad (M_{\rm cl}\ln\Lambda)(t) \;/\; M_{\rm bound}(t) \qquad (14)$$

The bound mass of the cluster is a quantity which is computed by SUPERBOX, the simulation programme used in this study, at each time-step of the simulation. In this routine an energy argument is used instead of determining the Roche radius. All particles having negative energy with respect to the cluster potential are flagged as bound. Measuring $\ln\Lambda$ according to Eq. 14 gives values which are systematically above the fitting line representing the cluster with a point-mass potential. But, using the above argument that an extended object should have a larger $b_{\rm min}$ than that with a point-mass potential, the tri-pods measured from this simulation would be systematically below the fitting line if the bound stars adequately account for all the mass which contributes to the dynamical friction. This disparity is a first hint that more particles may take part in the dynamical friction than just the bound stars. In the later stages of the evolution these values for $\ln\Lambda$ increase quite dramatically which is a clear sign that $M_{\rm cl}$ is underestimated.

In Fig. 6, we plot the bound mass of the object as a function of time (solid line). In the same figure, crosses and squares represent the mass of the cluster taking part in the dynamical friction process if we assume the same $\ln\Lambda$ as derived for a cluster with a point-mass potential and solve for $M_{\rm cl}$ with Eq. 7:

$$M_{\rm cl}(t) \quad = \quad (M_{\rm cl}\ln\Lambda)(t) \;/\; (\ln\Lambda)_{\rm pointmass}(t) \qquad (15)$$

For the crosses we apply the actual values from the point-mass simulation while the data-points of the squares are derived using the smoothed fitting curve for $\ln\Lambda(D)$ from Eq. 10. (Since we have already shown that the magnitude of $\ln\Lambda(D)$ for a cluster with a Plummer potential is smaller than that for a point mass potential, the actual total mass which contributes to the dynamical friction is slightly larger than both the values represented by the crosses and the squares.). Even though the uncertainties are large the data points show that the total mass which contributes to the effect of dynamical friction is systematically above the bound mass in the bound mass curve.

In addition to the bound mass we determine the lost mass of the cluster which is located in a ring of the cluster's extension around the galaxy at the same distance and only the particles with the same velocity signature as the cluster (orbital velocity $\pm$ velocity dispersion) are counted. Adding this mass to the bound mass is

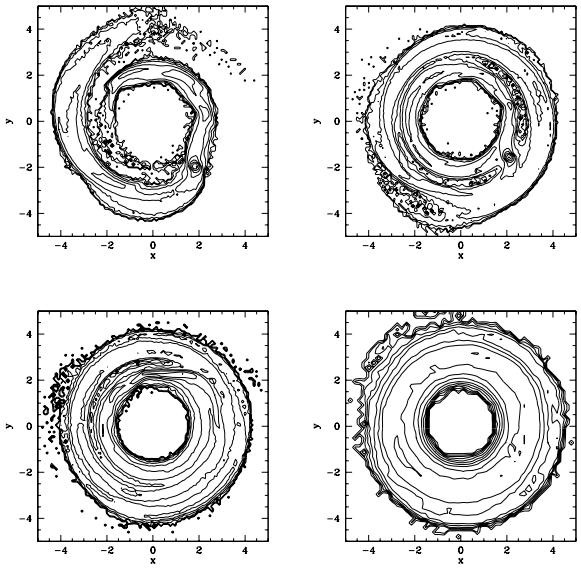

Figure 7. Contour plots of the time evolution of a star cluster larger than the tidal radius. Shown are the time-slices at 2.5, 5.0, 10.0, and 20.0 time-units.

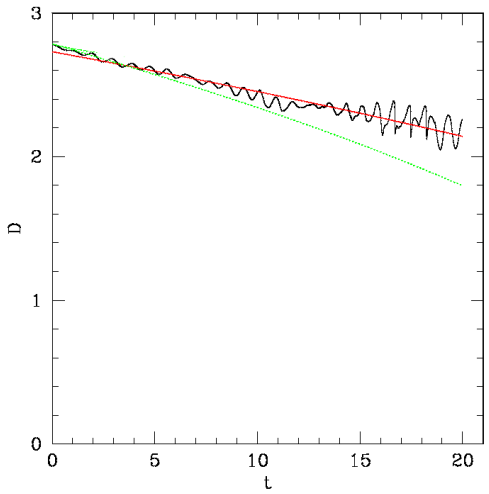

Figure 8. A diffuse star cluster which is larger than the tidal radius. The orbital evolution of the star cluster is plotted as a solid line (black). The dotted line (green) represents the maximum orbital decay rate derived for a cluster with a point-mass potential. (Red) solid line is the orbital decay with the actual values for $M_{\rm cl}\ln\Lambda$ inserted.

shown as the short dashed line in Fig. 6. This mass estimate seems to fit the data much better than the bound mass only. In an impulse approximation, the escaped cluster particles on the opposite of the galaxy do not contribute to the dynamical friction and should not be included in the active mass associated with the cluster. But, the cluster does have follow up encounters with the perturbed particles during either the present or subsequent orbits. The numerical results presented here is indicative that dynamical friction is a collective effect and not only the bound mass is responsible for it. To what extend the particles with large azimuthal separations from the cluster contribute to its orbital decay needs to be addressed in much more elaborate studies which may include alternative formulations (other than impulse approximation) of dynamical friction. Such an analysis may provide a weighting function to appropriately include the relatively weak contribution of the more distant particles.

We note a large fraction of the co-moving unbound mass is contributed by particles which became detached from the cluster in the previous orbit and are currently located within 2-3 Roche radii from the cluster. But attempts to use radial criteria like all particles within 2, 3 or 5 tidal radii or counting only leading/trailing arm particles (curves are not shown) were not successful in fitting the data. Thus, we applied a simple rule-by-thumb by adding half of the unbound mass to the bound mass (shown as long dashed line in Fig. 6). This simple estimate fits the data nicely taking into account that the 'actual' $\ln\Lambda$ of an extended object should be smaller than the one of a point mass, i.e. the data points have to be regarded as lower limits. But please keep in mind that this expression is just an *ad hoc* estimate without any rigorous derivation.

4.3 Diffuse star cluster with its cut-off radius larger than its tidal radius

Toward the end of the previous simulation, the compact cluster migrate toward the centre of the background galaxy where the external tidal perturbation is sufficiently strong to cause total disruption. In order to study the effect of the dynamical friction during the disrup-

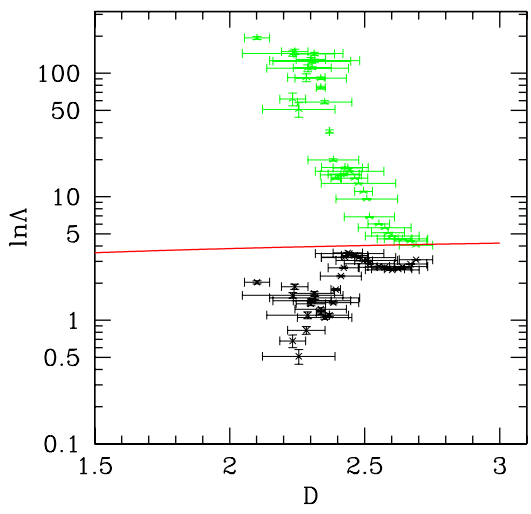

Figure 9. The deduced values of $\ln\Lambda$ from the simulation of a diffuse cluster with a cut-off radius larger than its tidal radius. Crosses (black) represent the values of $\ln\Lambda$ according to Eq. 13 and tri-pods (green) represent the values for $\ln\Lambda$ deduced from Eq. 4 under the assumption that $M_{\rm cl} = M_{\rm bound}$ (Eq. 14). The fiducial values of $\ln\Lambda$ for a cluster with a point-mass potential is also plotted for comparison purpose (red solid line). These data show that the assumption the bound mass clearly underestimates the total mass responsible for dynamical friction because the values of $\ln\Lambda$ increase to unphysical values.

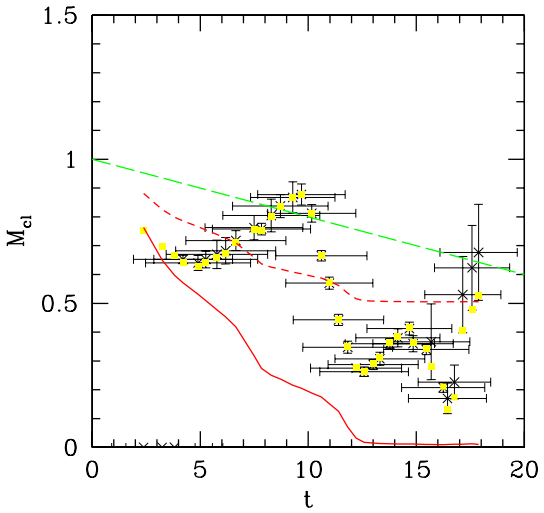

Figure 10. Mass evolution of a star cluster with an initial cut-off radius larger than its tidal radius. Solid line (red) is the bound mass as calculated by SUPERBOX. Again the crosses (black) and squares (yellow) are the values for the mass taking part in the dynamical friction process if $\ln \Lambda$ deduced for a cluster with a point-mass potential is applied (for explanation see Fig. 6). Long dashed line (green) represents all the stars in a torus with a width comparable to the initial size of the cluster at the distance of the cluster which have the same velocity signature as the stars within the cluster. Short dashed line (red) corresponds to the value of effective mass in accordance with our rule-by-thumb.

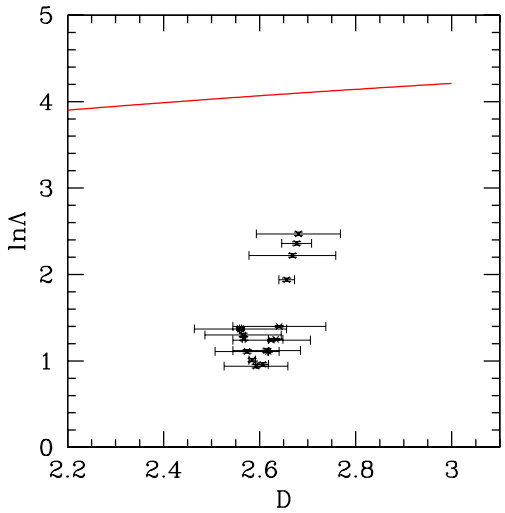

Figure 11. A moving cluster of unbound stars which only participate in gravitational interaction with the background stars. The mutual gravity between the cluster stars is neglected. (Therefore the cluster stars have no internal velocity dispersion but follow only the orbital motion at the beginning of the simulation). This figure shows the fitted values for $\ln \Lambda$ according to Eq. 13 for each 5 oscillations as function of the distance D to the centre of the background galaxy. Only a few data points are measurable before the cluster disperses completely. The data-points are well below that for a cluster with point-mass potential, which is shown as solid line (red). But the magnitude of $M_{\rm cl} \ln \Lambda$ is definitely not zero.

tion of the cluster, we carry out a third simulation with a star cluster having a stellar distribution extending beyond it tidal radius. For the initial cluster structure, we adopt a Plummer-sphere with Plummer-radius of $r_{\rm pl} = 0.1$ and a cut-off radius of $r_{\rm cut} = 0.5$. This cluster is launched on the same circular orbit as the previous simulations. It loses mass immediately and is destroyed after a few orbits around the background galaxy. With this set of initial conditions, we exaggerate the rate of tidal disruption of the cluster. Although this set of initial conditions seems to be unattainable, in some clusters (such as the Arches cluster), where the internal two-body relaxation may sufficiently intense, the outer regions of the clusters may be replenished on time scale shorter than their galactic orbital periods (McMillan & Portegies Zwart 2003). Most dwarf galaxies are on highly eccentric orbits with period comparable to their internal evolution time-scales. These systems tend to lose bound mass near their perigalactica where the tidal radius may also be reduced inside their cut-off radius. If this perigalacticon passage is brief compared to the internal time-scales the object does not have time to adjust smoothly to the mass-loss and is therefore in a similar state as our model.

In Fig. 7 we illustrate the orbital evolution of the star cluster. This figure clearly shows that already at time 10.0 there is no longer any distinctive density enhancement at the star cluster position. Nevertheless, we are able to determine the centre of density of the last percents of bound particles and trace its orbit. Fig. 8 shows that the remains of the object still sink to the centre even after the tidal disruption of the cluster is nearly completed. Beyond time 15.0 the determination of the centre of density of the residual star cluster becomes very difficult and highly uncertain. But there still are indications that the remnant core continues to undergo orbital decay even after its near complete disruption.

In Fig. 9 it is visible that in this case the assumption that only the bound mass is responsible for dynamical friction is no longer valid. Instead of staying close to the values determined in the point-mass case the values of $\ln \Lambda$ according to Eq. 14 keep on increasing to really unphysical values of more than 200.

Following the analysis for the previous model, we use the value of $\ln \Lambda$ which was determined for a cluster with a point-mass potential to derive a mass which is responsible for the dynamical friction. This mass-estimate is shown in Fig. 10 as crosses and squares. The values of this mass are clearly above the line of the bound mass and below the line of the particles inside the ring of the star-cluster orbit with the same velocity-signature. They approximately correspond to the bound mass plus half of the mass which is already lost (our rule-by-thumb).

4.4 A moving cluster without self-gravity

We provide additional evidence that the recently-detached stars contribute to the process of dynamical friction. We construct an artificial demonstration in which the mutual gravity among the stars associated with the cluster is neglected. In this construct, none of the cluster particles are bound to each other but the gravitational interaction between them and the background stars is preserved.

With this prescription, the cluster stars begin to disperse almost immediately. But, we are able to follow the orbital evolution of the density centre for several orbits. Following the previous analysis, we determine $M_{\rm cl} \ln \Lambda$ and plot the derived values against the mean distance to the centre in Fig. 11. These values are well below the analogous values for the cluster with a point-mass potential.

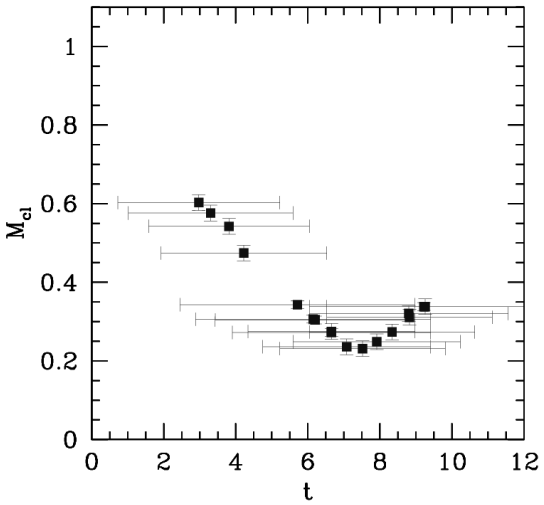

Figure 12. Applying $\ln\Lambda$ from the point mass simulation and calculating the mass taking part in the dynamical friction process as a function of time. In the beginning the data points are spread around half of the cluster mass, which is a verification of our rule-by-thumb (Here the whole mass of the cluster is unbound from the onset of the simulation, therefore the mass for dynamical friction should be half of the cluster mass.). At later times the moving cluster disperses more and more and the values start to drop.

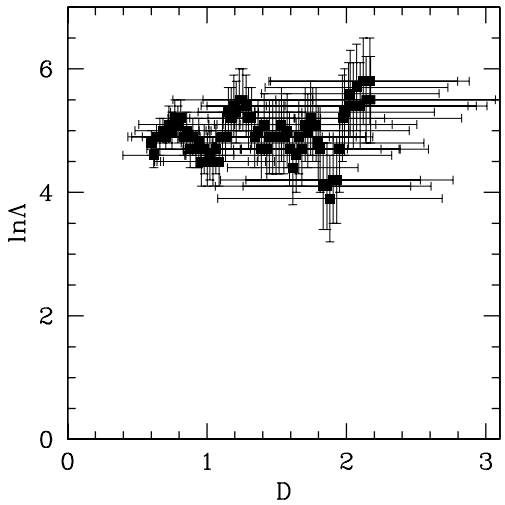

Figure 13. Point-mass star cluster on an eccentric orbit. Shown are the derived values for $\ln\Lambda$ in the point-mass case plotted against the mean distance of the cluster to centre of the galaxy (according to Eq. 16). Because of the eccentricity of the orbit the uncertainties in D are quite large (error-bars denote the maximum and minimum distance to centre during 5 oscillations which are used to determine $\ln\Lambda$).

Based on the assumption that the simulation for the cluster with a point mass potential provides a reliable value of $\ln\Lambda$, we determine the mass $M_{\rm cl}$ responsible for dynamical friction of this moving group in Fig. 12. Even though the bound mass of this moving group is actually zero from the onset of the simulation, the coherent movement of the cluster particles can induce dynamical friction. At the beginning approximately half of the cluster mass is involved which proves again our rule-by-thumb and only later the particles become too disperse and this mass is reduced.

4.5 Cluster on an Eccentric Orbit

Finally we examine the nature of the oscillations which are apparent in Figs. 6, 10 & Fig. 12. These oscillations do not show any preferred period and are longer than and not related to the orbital time-scale of the cluster. These oscillations appear to be caused by the enhanced dynamical friction associated with the close encounters between the residual cluster and the stars which became detached during previous orbits and have wrapped around the galaxy to the vicinity of the cluster. In our model setup this wrap-around happens already in the very early stages (after 3-4 orbits) of the simulations as shown in Figs. 3 & 7. The trailing and leading debris have local density variations which can lead to variations in their perturbation on the motion of the residual clusters. As a test for this conjecture, we placed a cluster on an initial eccentric orbit. In the gravitational field of the background galaxy, the galactic orbit of the cluster and its debris diverge due to differential precession and the relatively large velocity differences between the residual cluster and the wrapped around debris stream limits the influence of the detached stars on the orbital evolution of the residual cluster.

Following previous procedures, we first carried out a simulation with a cluster with a constant point-mass potential. The cluster orbit has an initial eccentricity of 0.4 and an orbital period of 0.74.

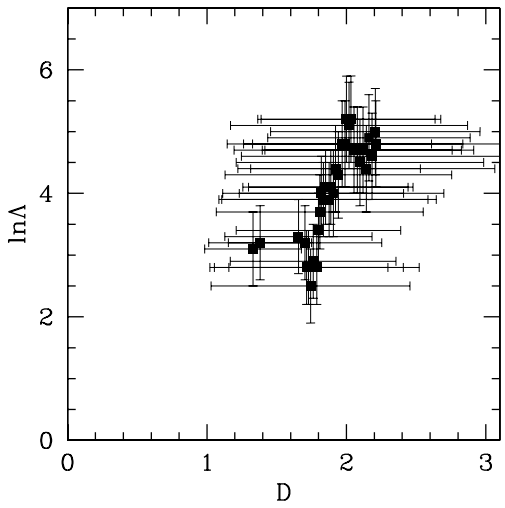

Figure 14. Compact star cluster on an eccentric orbit. Shown are the values for $\ln\Lambda$ for the star cluster. The cluster used in this simulation is the identical model which is used for the cluster smaller than the tidal radius case with circular orbit. The values for $\ln\Lambda$ are derived if we assume $M_{\rm cl} =$ const.$= 1.0$. (see Eq. 13)

We derive the values of $\ln\Lambda$ as a function of cluster's mean distance from the galactic centre, which is now computed as

$$D \quad = \quad (\langle D_{\rm apo}\rangle + \langle D_{\rm peri}\rangle)/2 \qquad (16)$$

for each time-slice which covers 5 orbits around the centre of the background. A comparison between Fig. 13 and Fig. 2 indicates that the value of $\ln\Lambda$ for the same value of D is somewhat larger for a cluster with an eccentric orbit than that with a circular orbit.

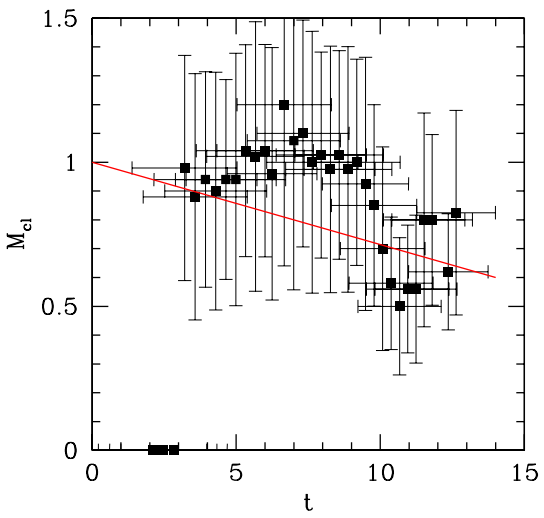

Figure 15. Compact star cluster on an eccentric orbit. Shown is the mass responsible for the dynamical friction if we adopt the values for $\ln \Lambda$ from the point mass case (eccentric orbit; see Fig. 13). Solid line (red) denotes the bound mass of the cluster. The simulations with eccentric orbits were performed to investigate if the mass responsible for the dynamical friction shows similar 'oscillations' than in the circular orbit simulations. The values still show the same kind of long-period oscillations, but they are now smaller than the actual uncertainties of the mass.

The modest epicycle amplitude expands the radial range of halo stars which respond to the gravity of the cluster with an eccentric orbit than that with a circular orbit. This effect corresponds to an increase in the magnitude of $b_{\max}$ in Eq. 2.

Fig. 14 displays the corresponding values for a compact star cluster with the same eccentric initial galactic orbit as that for the point-mass potential test model. We used the same Plummer stellar phase space distribution for the compact cluster as described in Sect. 4.2. In this case, the cluster's cut-off radius is smaller or larger than its tidal radius near its initial apogalacticon or perigalacticon respectively. Under the assumption that all of its initial mass contributes to the effect of dynamical friction, the magnitude of $\ln \Lambda$ for the active cluster is smaller than that of a cluster with a point-mass potential. This disparity is consistent with the results obtained in Sect. 4.2 and it is particularly notable at relatively small D where a significant fraction of the cluster is lost.

Using the values of $\ln \Lambda$ derived for the cluster with a constant point mass potential (see Fig. 13), we estimate the total cluster mass which contributes to the process of dynamical friction. The results are plotted as dots with error bars in Fig. 15. For comparison, we also plotted evolution of the mass which remains bound to the cluster. This quantity is computed self consistently from the relative total energy of each particle with respect to the cluster. It is plotted as a solid (red on-line) line. The bound mass appears to be less than the total mass which contributes to the effect of dynamical friction. It is also notable that the amplitude of long-term oscillation in $M_{\rm cl}$ is significantly reduced. Toward the end of the simulation (at $t > 10$), the effective mass also becomes comparable to the bound mass which may also be due to the orbital divergence of the debris from the parent cluster.

5 CONCLUSIONS

Dynamical friction is an important process which determines not only the rate but the outcome of dynamical evolution of satellite stellar systems in the halo of large galaxies. The total mass of compact satellites is preserved while they orbit around the outer halo with cut-off radii smaller than their tidal radii. These entities undergo orbital decay and encounter increasingly strong external tidal perturbation. The time scale of the orbital evolution is determined by the magnitude of both the mass and $\ln \Lambda$ which itself decreases with the slope of the density fall off at outer regions of the satellite. Due to the enhanced effect of close encounters, the magnitude of $\ln \Lambda$ for a cluster with a point mass potential increases with the numerical resolution. However, for clusters with a realistic density distribution, the magnitude of $\ln \Lambda$ converges in the high resolution limit and it can be reliably measured in the limit of negligible mass loss.

As satellite stellar systems undergo orbital decay, they encounter increasingly strong tidal perturbation from their host galaxies. Stars in the outer regions of loosely bound clusters and dwarf galaxies become detached and form a tidal debris. But the orbits of these detached stars do not change abruptly and they diffuse away from the vicinity of their parent clusters or dwarf galaxies on the orbital time scales. Near the tidal radius of their parent clusters and dwarf galaxies, individual detached stars exchange momentum and energy with the dark matter halo at comparable rates as the bound stars. Even though they are already detached, the escapers continue to maintain modest gravitational interaction with the bound stars such that they contribute to the collective dynamical friction effect.

In this paper, we provide a numerical model of a cluster which is undergoing tidal disruption. By fitting the simulated orbital decay with conventional formulae, we show that the residual bound stars alone cannot fully account for the rapid rate of orbital decay induced by dynamical friction. We show that particles which become recently unbound but remain close to the object also contribute to the effect of dynamical friction. In our 'realistic' model, the evidence for this effect is systematically shown with a considerable amount of uncertainty during the initial stage of mass loss. But this general result is enhanced dramatically during the last phases of the dissolving process. Our model star clusters continue to undergo orbital decay even after all particles have already become unbound. Due to the fact that our code is able to use millions of particles we are able to trace the density enhancement of the dissolved star cluster for quite some time after its dissolution and we found that this moving cluster of unbound stars continue to undergo orbital decay.

We propose that the mass responsible for dynamical friction is the sum of that in the cluster and a large fraction of the mass of the stars in the tidal debris which follow similar orbits. The additional mass to be taken into account are those stars which have the same velocity and are contained in a ring centred on the cluster's original orbit and with a half width comparable to the original radius of the parent cluster. Our results differ slightly from the findings of Fujii et al. (2006) who suggested that only the trailing arm and the unbound stars in the direct vicinity enhance the dynamical friction. Our results are in better agreement with taking both leading and trailing arm into account, as long as the particles are in a similar orbit as the remaining satellite. Still, regarding the large error-bars, our data-points agree with a simple rule-by-thumb (which has no physical explanation). We have shown that one has to take approximately half of the mass which is lost into account. This rule-by-thumb is valid at least as long as we could trace the orbit of our models and is similar in a quantitatively way to the

findings of Fujii et al. (2006). This simple rule-by-thumb remains valid even after the cluster has become completely tidally disrupted into a moving cluster of unbound stars.

While the results from this study and from Fujii et al. (2006) during the dissolution phase are very similar, we are able to trace the decay of the satellite even beyond the total destruction, (at which stage Fujii et al. (2006) stop their simulations). We showed for the first time that a satellite which exists only as a moving cluster of an unbound density enhancement still suffers dynamical friction and sinks towards the centre of the host system.

This result has some major implications for recent astronomical questions. It increases the possible distance range of the birth place of the central star cluster in our Milky Way. In the case of star clusters sinking to the Galactic Centre during their very short lifetimes this result could alter the conclusion of a study. Especially the fact that dissolved clusters continue their orbital decay at least for a few orbits really enhances the parameter range from where the central stars were from.

Tidal debris are found around many satellite galaxies in the Galactic halo. For example, the mass estimated for the stellar stream associated with the Sagittarius dwarf spheroidal galaxy is more than an order of magnitude larger than the total residual mass within that galaxy (e.g. Helmi 2004; Law et al. 2005; Fellhauer et al. 2006). The Magellanic stream, which is mainly composed of neutral hydrogen, also has a mass which is more than a few percent of that in the Large Magellanic Cloud (e.g. Lin & Lynden-Bell 1977, 1982; Connors et al. 2006). There are also suggestions that several satellite dwarf galaxies lie on various great circles in the sky (Lynden-Bell & Lynden-Bell 1995) perhaps as debris of much larger entities. In this context, our results also imply that during their tidal disruption, the orbital decay of dwarf galaxies in the Galactic halo is sustained at a rate much larger than that extrapolated from their instantaneous declining mass. The contribution of detached stars enhances the strength of the dynamical friction and promote the completion of the dwarf galaxies' tidal disruption. Without it, the orbital decay of the dwarf galaxies would be halted while many remnant cores would be preserved. This process provides a possible scenario to attribute the "missing satellite" problem to their enhanced dynamical friction and effective tidal disruption.

There have been many attempts to reconstruct the orbital evolution of the dwarf galaxies from their present-day properties. Our results suggest that these models may need to be modified to take into account the efficient dynamical friction, especially during the epoch when a substantial fraction of their halo dark matter has already become detached from the satellite galaxies. Our results also indicate that the current location where the tidal debris are found may not necessarily be the location where they became detached from their host satellite galaxies.

The most and second most massive globular cluster around the Galaxy are ω-Cen and M22. The metallicity dispersion within these cluster is in strong contrast to all other cluster. But similar metallicity dispersion has been observed in dwarf spheroidal galaxies (McWilliam & Smecker-Hane 2005). It has been suggested that these clusters may be the cores of disrupted dwarf spheroidal galaxies. M22 actually resides in the central region of the Sagittarius dwarf spheroidal galaxy. The results we have presented above provide supporting evidence that dynamical friction is efficient in inducing satellites' orbital decay, especially during the break-up stage when a large fraction of the original mass, either in the form of stars in the outer envelope or loosely found dark matter, become detached from the residual satellite galaxies. The enhancing contribution from the break-up stars may indeed have promoted the disruption of the original parent galaxy and deposit its nucleus (ω-Cen) at the position where it is found today.

We thank Dr. R. Spurzem for useful conversation. This work was supported in part by NASA (NAG5-12151) and the California Space Institute.

REFERENCES

Bekki K., Freeman K.C., 2003, MNRAS, 346, 11L
Belokurov V., et al., 2006a, ApJ, 642, 137L
Belokurov V., et al., 2006b, ApJ, in press
Belokurov V., Evans N.W., Irwin M.J., Hewett P.C., Wilkinson M.I., 2006, ApJ, 637, 29L
Binney J., Tremaine S., 1987, Galactic Dynamics, Princeton University Press
Blumenthal G.R., Faber S.M., Primack J.R., Rees M.J., 1984, Nature, 311, 517
Chandrasekhar S., 1943, ApJ, 97, 255
Connors T.W., Kawata D., Gibson B.K., 2006, MNRAS, in press
Fellhauer M., Kroupa P., Baumgardt H., Bien R., Boily C.M., Spurzem R., Wassmer N., 2000, NewA, 5, 305
Fellhauer M., et al., 2006, ApJ, in press
Fujii M., Funato Y., Makino J., 2006, to appear in PASJ, astro-ph/0511651
Gerhard O., 2001, ApJ, 546, 39L
Hashimoto Y., Funato Y., Makino J., 2003, ApJ, 582, 196
Helmi A. 2004, ApJ, 610, 97L
Hilker M., Richtler T., 2000, A&A, 360, 895
Ibata R.A., Lewis G.F., Irwin M.J., Quinn T., 2002, MNRAS, 332, 915
Just, A., Penarrubia J., 2005, A&A, 431, 861
Krabbe A., et al., 1995, ApJ, 447, 95L
Law D.R., Johnston K.V., & Majewski S.R. 2005, ApJ, 619, 807
Lin D.N.C., Lynden-Bell D., 1977, MNRAS, 181, 59
Lin D.N.C., Lynden-Bell D., 1982, MNRAS, 198, 707
Lynden-Bell D., Lynden-Bell R., 1995, MNRAS, 275, 429
McMillan S.L., Portegies Zwart S.F., 2003, ApJ, 596, 314
McWilliam A., Smecker-Hane T.A., 2005, ApJ, 622, 29L
Martnez-Delgado D., Gmez-Flechoso M.A., Aparicio A., Carrera R., 2004, ApJ, 601, 242
Moore B., Ghigna S., Governato F., Lake G., Quinn T., Stadel J., Tozzi P., 1999, ApJ, 524, 19L
Navarro J.F., Frenk C.S., White S.D.M., 1995, MNRAS, 275, 56
Odenkirchen M., et al., 2003, AJ, 126, 2385
Penarrubia J., Just A., Kroupa P., 2004, MNRAS, 349, 747
Spinnato P.F., Fellhauer M., Portegies Zwart S.F., 2003, MNRAS, 344, 22
Tamblyn P., Rieke G., 1993, ApJ, 414, 573
Tsuchiya T., Korchagin V.I., Dinescu D.I., 2004, MNRAS, 350, 1141
Willman B., et al., 2005, ApJ, 626, 85L
Zucker D.B., et al., 2006a, ApJ, 643, 103L
Zucker D.B., et al., 2006b, ApJ, submitted